# CHAPTER 1

# MODELING FOR MEDICAL IMAGE ANALYSIS: FRAMEWORK AND APPLICATIONS

MAREK KRĘTOWSKI

*Faculty of Computer Science, Bialystok Technical University*
*Wiejska 45a, 15-351 Bialystok, Poland*
*mkret@ii.pb.bialystok.pl*

JOHANNE BÉZY-WENDLING

*LTSI, INSERM, University of Rennes I*
*Bat. 22, Campus Beaulieu, 35042 Rennes Cedex, France*
*johanne.bezy@univ-rennes1.fr*

In the chapter, we discuss how medical image analysis can take advantage of computational modeling. First, a general framework of model-based approach is presented, whose objective is enabling to relate external descriptions to internal processes, which originate them. Two coupled models *i.e.* model of an organ under study and model of an imaging modality, constitute main components of this framework. Then, a few applications of the presented approach are described. Two vital abdominal organs, namely liver and kidney, are considered and their typical pathological processes connected with significant vascular modifications are analyzed. Resulting patterns are observed by means of dynamic Computed Tomography, when contrast material injection and propagation are simulated. Texture features are extracted from regions of interest defined in simulated images in different acquisition conditions. Studying evolution of features allows us to better understand both advantages and limitations of texture analysis and is very helpful in proper medical image interpretation.

*Keywords*: Computational modeling; vascular network; image simulation; biphasic computed tomography; compartmental model; hepatic enhancement; texture analysis

## 1. Introduction

Modeling is an extremely wide field where each discipline can find its place by adapting the generic concepts to the building of its own models. A very complete theory of modeling and simulation is given in Ref. 1. In this chapter, we confine

C.T. Leondes (Ed.) *Medical Imaging Systems Technology: Analysis and Computational Methods* (vol. I), pp. 1-32, 2005. 

ourselves to the field of life sciences, and more especially to medical imaging. In biology and medicine, some observation systems allow analyzing finer and finer phenomena, which are really the disease causes and not only its anatomic and functional consequences. Indeed micro-imaging modalities provide insight into cells, chromosomes and genes[2]. However, non invasive examinations realized in clinical routine are generally still macroscopic, and they are used to detect and characterize a disease, through markers that generally are a complex mixture of parameters situated at inferior physiological levels. Going from one level to the other one is a key point in the early detection of pathology, and therefore in the definition of an efficient treatment. It then constitutes a main issue and it is the objective of a great number of works in the biomedical field.

*Modeling* can participate to the setting up of bridges between these different observation levels, by extracting, at the macroscopic level, information representative of the level capable of explaining pathology[3]. This task can be achieved only if the abstraction level of the model is well chosen[4]. Parameters related to the physiological phenomena one wants to analyze and to understand, have to be integrated in the model. One of the main difficulties in a model design is the necessity to capture the essential properties of the system, without dealing with elements whose role is minimal in its functioning. These essential elements are not always identified before the model conception, and may be revealed during its definition. This is especially the case for living systems whose structural and functional *complexity* is generally great. This complexity is due to the important number of components (all the more numerous since the level of description is high) and to their connections.

*Methodology* of modeling is chosen taking into account the knowledge we have on the physiological system and the way we want to use the model. For instance, the approach for generating the model will be different if the objective is to explain the system functioning, or only to reproduce it[5]. In the first case, a *"knowledge based"* model will be designed by considering *a priori* knowledge (i.e. physical and physiological principles followed by the system), modeling purpose and experimental data. In the second case, the *"data driven"* or *"black box"* model is derived from collected experimental data, and consists in a mathematical description of the system, without explicit correspondence with underlying physiological processes.

In both preceding cases, a simulator is used to generate the model behavior. *Simulations* are useful during the model building, to precise its structure or adjust parameters. This is the necessary step of model *validation*. Several definition of validity can be found. Zeigler says that a model is valid (replicative validity) if "for all the experiments possible within the experimental frame, the behavior of the model and system agree within acceptable tolerance"[1]. In the field of biology and medicine, the validity of a model can be sometimes difficult to assess because data collection can be impossible or very difficult to realize. When the model is completed and validated, simulations are used in order to better understand the system, and especially how it would work in particular conditions that can not be

easily tested in reality (prediction).

System specification formalisms are proposed in Ref. 1 considering continuous and discrete systems. Simulators are also presented for these approaches. In Ref. 5 Carson and Cobelli introduced a methodology for the development of mathematical models in physiology and medicine. It is illustrated, for instance, on modeling circulatory and respiratory systems. Mathematical models of physiological systems (circulatory, respiratory, renal, muscular, neural) and population dynamics are also described in Ref 6.

In this chapter we present a model-based approach to medical image analysis, whose objective is to relate external descriptions to internal processes or systemic behaviors, which originate them. A general framework[7] corresponding to this approach is displayed in Fig. 1.

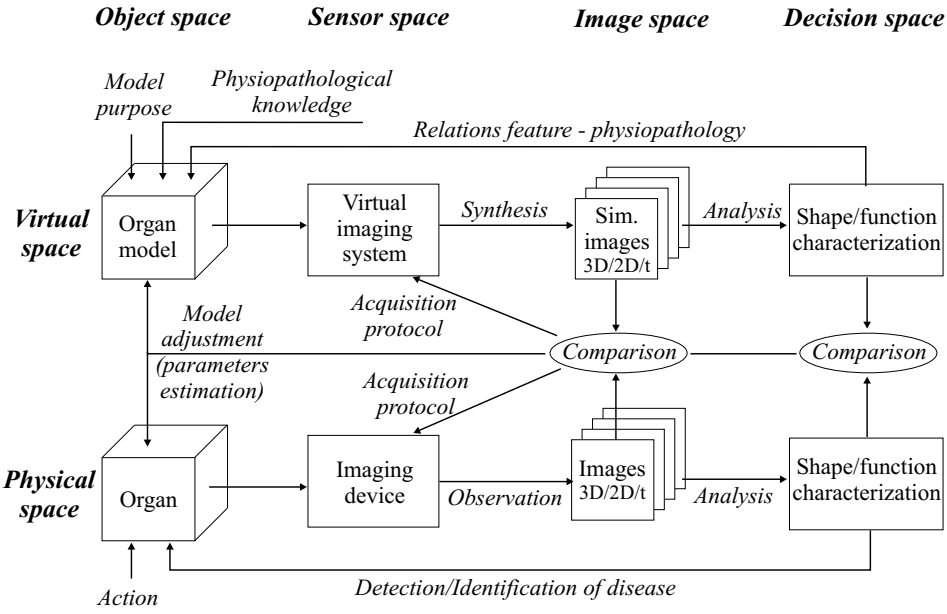


Fig. 1. General framework of model-based approach to medical image analysis.

Any attempt devoted to design in-depth model-based representations, as opposed to more widely used external descriptions, has to rely on the basic mechanisms originating the objects (*i.e.* tissues, organs or systems) under study, the environmental conditions in which they develop (*i.e.* functional interactions and spatial constraints for instance) and the deviations that can occur during their formation or after (reflecting inter-individual variations as well as pathological evolutions). All these features are included into the "object space" depicted in Fig. 1. The sensing device, specified here as "virtual imaging system" must also be modeled in a real-

istic way in order to simulate sound images. This task involves taking into account the physical principles of the imaging modality and the image reconstruction algorithms (both being merged into the "sensor space") leading to image formation as well as the distortions they both convey. Any imaging device can be considered according to the organ properties to be analyzed. These two objectives are very challenging as such but it is the only way to get a really relevant "image space". So produced virtual data can then be submitted to any image analysis method capable to answer to the given objectives. Such processing can be oriented toward morphological or structural studies and focused, among many others, on segmentation and characterization tasks (static 2D or 3D images). They can deal with functional features when time stamped images are generated (i.e. time image sequences) using motion estimation or compartment models when they are of concern. The overall system output belongs to what is called the "decision space", which may rely on any pattern recognition methods (statistical data analysis, neural networks, ...). From this standpoint, a full matching, where the same views operate, can be proposed by considering the "virtual space" and its dual, the "physical space".

A number of highly meaningful concepts can then be projected onto this 2 by 4 matrix. A few ones (classical feedback being still valid) are exemplified here. The first one corresponds to the capability at each step to compare the real and virtual outcomes either at a visual level or through quantitative characteristics. For example, local and global statistical measures can be performed on the simulated as well as on *in-vitro* or *in-vivo* data. They can bring new cues for model building and adjustment (initialization conditions, error criteria, ...). Similar feature extraction (distances, volumes and shape descriptors, ...) can be achieved into the image planes issued from virtual and physical imaging devices.

The second concept emphasizes the possibility to link directly the decision space (and the extracted features) to relevant pathophysiological patterns: this opens the road towards explanative analysis or physiologically founded understanding of image features. It allows replacing formal parameters by variables with a structural or functional meaning. Direct or inverse problems are here of main interest if it can be proven that the corresponding system is identifiable. However, a pragmatic solution consisting in estimating the linear or non linear relations between the measures and the underlying, fully controlled, physiological variables can be of value in the first step.

Moreover, through these simulation capabilities, the impact of changing the acquisition parameters (for instance the spatial resolution, the time windows and delays) on the "decision space" can be objectively anticipated. For instance, instead of making use of simple shaped phantoms with additive noise to evaluate the performances of detection, segmentation, reconstruction algorithms among others, realistic objects with varying observation conditions can lead to more robust conclusions. Appropriate protocols can then be derived in a predictive way.

To summarize, model-driven acquisition, analysis and interpretation are offered

by such a generic frame. Of course, its relevance goes well beyond the imaging field here addressed. The same views can be applied to model-based signal processing[8] or biology[9]. An instantiation of this conceptual approach will be described in the following sections. The object is then the abdominal organ with its vascular network which is modeled at each step of its development, with structural, morphological and functional information. The selected sensing device is a standard Computed Tomography scanner providing 3D observations and time-stamped image sequences when contrast material propagation is considered. The image analysis deals with texture characterization (emphasizing the need for feature meaning).

## 2. Model-based approach for image understanding

Modeling almost always means simplification and specialization. It should be emphasized that the presented organ model is oriented toward image generation and cannot be treated as a general purpose model of the organ. The proposed model is concentrated on elements which are directly visible on images or are closely related to the pattern formation process. Vessels play the key role in a contrast material propagation and they are one of the most visible structures on dynamic CT scans of abdominal organs. It is why the vascular system is very important component of the organ model.

### 2.1. *Physiological organ modeling*

In its generic form, the model is designed to simulate the development and pathological changes of extensive, parenchymous organs. It is assumed that such organs are able to increase their size during the growth phase by consecutive divisions of structural units (process of *hyperplasia*)[10].

The organ model consists of two main components: the tissue and the vascular network that perfuses it, and adapts to its local geometry. Most of model features are not linked with any particular organ, however, when we deal with the given organ some kind of specialization can be necessary to properly express its specificity. Liver is a good example of such a situation, because of its unique organization of the vascular network with three trees: hepatic artery, portal vein and hepatic vein.

The changes in the size and the structure of the organ and the corresponding vascular structures operate at discrete time instants called cycles (and subcycles). The overall flow chart (Fig. 2) depicts the main events, which can be distinguished in the model realization of the organ development process.

#### 2.1.1. *Tissue modeling*

Tissue is represented by a set of *Macroscopic Functional Units* (MFU) distributed inside a 3D volume, which constitutes external organ shape. This shape can be defined analytically or can be reconstructed (*e.g.* based on series of CT scans). Two phases (*growing phase* and *adult phase*) can be distinguished. They are directly

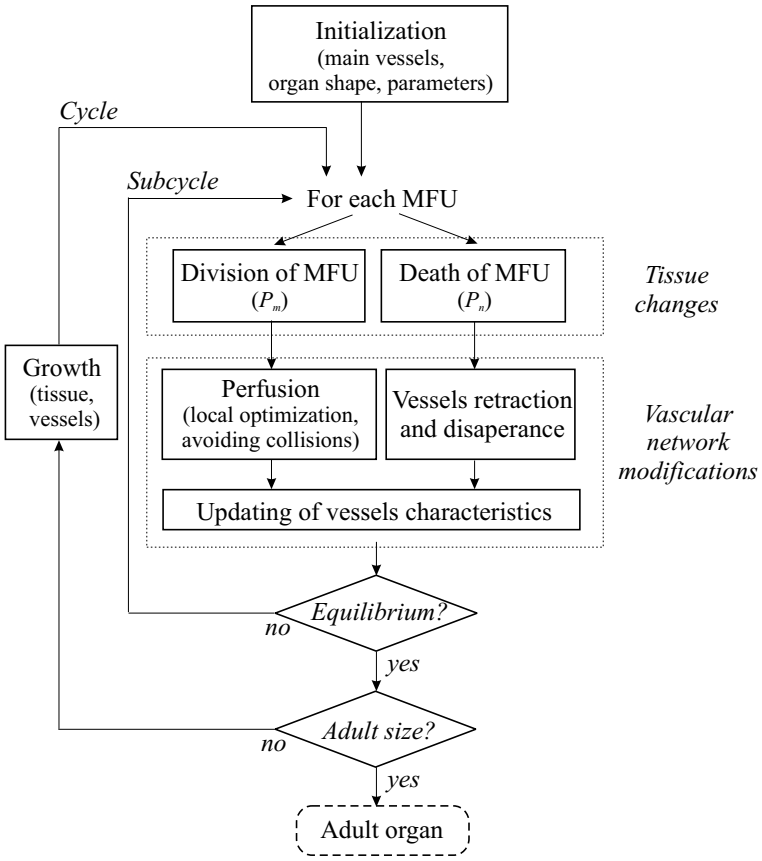


Fig. 2. Flow chart representing two loops of events which are distinguished in modeling of the organ (tissue and vascular network) development.

connected with the shape size changes. In the growing phase, the process starts with an organ, whose size is a small fraction of the one of an adult organ, and which expands gradually until it reaches the maximum size. In this moment the adult phase starts and the size of the organ remains invariable. Concerning the first phase, there exist a few possible ways of generating growing organ envelopes. The most precise one would use series of real data acquired at different ages, which is however hard to achieve in clinical practice. Therefore a single exam is processed to reconstruct the adult organ, which is then transformed to create the smaller shapes. This can be performed by either mathematical morphology operations (erosion, dilation) or simple scaling.

MFU is a small, fixed size part of the tissue, which spatial position is given relatively to the shape and does not change with the organ growth. Most of functional and structural properties of MFU are defined by its class *e.g.*:

- probabilities of mitosis $P_m$ and necrosis $P_n$, which are essential in the proliferation process. Usually $P_n$ is lower than $P_n$, especially when the organ is young. In fact, both probabilities are sensitive to time and they decrease with the age of MFU (exponentially decreasing functions)[11].
- metabolic needs (blood flow rate),
- blood pressures,
- density, which is closely linked to attenuation coefficient calculated during virtual imaging,
- size and other geometrically oriented parameters.

Certain parameters associated with the MFU class are described by their distribution and they are randomly chosen for each new MFU. This mechanism allows modeling the natural variability of the terminal blood flow in MFUs.

Several classes of MFUs are defined to differentiate functional (or pathological) regions of the tissue. For example, in normal kidneys one class corresponds to cortex and the other to medula.

In normal conditions, the class of MFU generally remains unchanged during all the life of the MFU, but in pathological situations this is not the case. A mechanism of conversions was introduced into the model to enable an initialization of the distinct region by a substitution the MFU class. Each conversion represents the period when the current class of MFUs inside the defined volume (*e.g.* sphere) can be changed (with the given probability) to another class. Conversions can be arranged in sequences and can also operate in a parallel way. The sequence of conversions enables to simulate for example various stages of lesion development, when characteristics of infected region evolve gradually in time. Moreover, parallel conversions operating in separate parts of the organ allow modeling multiple lesions (*e.g.* spread of tumor in form of metastasis). After the initialization of the pathological region by using conversion mechanism, the disease develops leading to changes in the vascular system of the organ.

### 2.1.2. *Vascular network modeling*

Individual parts of the whole vascular system are very diverse and their specificity should be taken into account during the modeling[12]. For example, transportation function dominates in main arteries delivering blood to organs and geometry of vessels is highly dependent on anatomy of the organism. Another situation can be observed in case of perfusion of abdominal organs like kidneys, where the most important task is filtration. In such a case location of specific vessels is not crucial, but spatial vessels density must be high enough to enable functioning of the organ.

There exists several vascular models and they differ considerably from one to the other. The models concern different organs and they were designed with completely distinct aims and level of details. One of the first proposals based on physiological mechanisms was described by Gottlieb[13]. As a result of an iterative algorithm

inspired by angiogenesis process a fractal structure of a vascular tree is created. This model was then refined and formalized in Ref. 14. Schreiner and Buxbaum proposed another method for an arterial tree generation, which they called Constrained Constructive Optimization (CCO)[15]. The tree develops by sequentially adding new bifurcations to the existing vascular structure. The optimal position of bifurcation point is searched to minimize volume of the whole tree.

Recently aforementioned two-dimensional models were replaced by much more realistic three-dimensional models. The one proposed by Bézy-Wendling[11] enabled growth of an arterial tree inside simple, analytically defined and gradually expanding volume[16]. New simulated cells, which appear during the growth of the organ, are perfused sequentially by newly created vessels. In Ref. 17 CCO method was extended in order to model an arterial tree development inside a 3D volume imitating an organ. Improved CCO was applied to simulate the coronary artery.

In the presented model, each vessel segment (part of vessel between two consecutive bifurcations) is represented by an ideal, rigid tube with fixed radius, wall thickness and position. It was assumed that the wall thickness depends on vessels diameter and its function (arteries have thicker walls than veins). In the model, all vessels until the level of capillaries are distinguishable. On the contrary the geometry of capillaries is not considered, these smallest vessels being "hidden" in the MFU. Based on morphometrical investigation dealing with bigger vessels (*e.g.* conducted by Zamir[18]), it is assumed that a single vascular structure has a form of a binary tree (Fig. 3). It means that anastomosis, which occurs sometimes, especially in pathological situations, cannot be modeled.

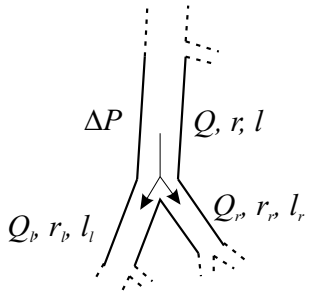


Fig. 3. A binary vascular tree is composed of successive bifurcations.

One of the most important assumptions concerns the blood flow. Blood is regarded as a Newtonian fluid with constant viscosity ($\mu$), whose flow is governed by *Poiseuille's law*:

$$\Delta P = Q\frac{8\mu l}{\pi r^4}, \tag{1}$$

where $P$ - stands for blood pressure, $l$ - vessel length, $r$ - radius. It enables to

calculate the difference of blood pressure between the ends of segment based on blood flow and geometry of the vessel. The physical law, which has to be verified at each bifurcation, is the elementary law of *matter preservation*:

$$Q = Q_r + Q_l, \tag{2}$$

where $Q_l$ ($Q_r$) denotes the blood flow in left (right) descendant vessel respectively. It means that the quantity of blood, which enters a bifurcation by the father vessel, leaves it by the two sons vessels. Another constraint that has to be fulfilled in the bifurcation deals with radii of vessels. This relationship was established empirically and is known as the *bifurcation law*:

$$r^\gamma = r_r^\gamma + r_l^\gamma, \tag{3}$$

where $r_r$ ($r_l$) denotes radius of right (left) descendant vessel respectively and $\gamma$ varies between 2 and 3 [19,18]. Based on this observation it is possible to estimate the radius of the ancestor vessels using radii of descendant vessels.

Assuming that positions of all vessels are fixed, it is necessary to assure the consistency of the characteristics (*i.e.* blood flow and pressures, ...) describing individual vessels. The vascular tree is consistent if: *i)* it has the same blood pressure and fixed blood flow in all terminal vessels attached to MFUs, *ii)* the Poiseuille law in each vessels, matter preservation and bifurcation laws in each bifurcations are fulfilled. A computationally effective method for the consistency assurance in the vascular tree is described in Ref. 20.

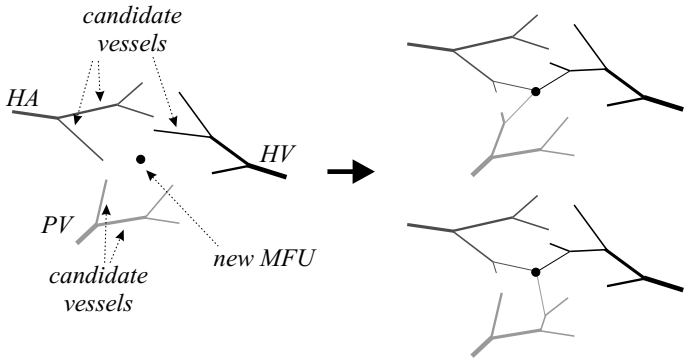


Fig. 4. Perfusion process of newly created MFU by hepatic vascular network. The optimal configuration of vessels is chosen depending on minimal volume principle.

Newly appeared MFUs are initially ischemic, because they are not perfused by the existing vascular network. The MFU signals this by secreting some angiogenic factors. In response to this biochemical stimulus the closest vessels (called candidate vessels) sprout toward the source of the stimulation. The stimulation disappears when the first vessel (in each tree) reaches the MFU and consequently remaining

new vessels retract. Geometry of a newly created bifurcation is controlled by local minimization of additional blood volume needed for the MFU perfusion. In order to find out the optimal configuration, each candidate vessel temporarily creates a bifurcation perfusing the MFU and the configuration volume is calculated (Fig. 4). Additionally, the problem of avoiding possible collisions between perfusing vessels has to be taken into account. It concerns both intersection of vessels coming from the same tree and also, what is especially important, crossing among arteries (arterioles) and veins (venules). In the adapted, simple approach, only non-crossing configurations are considered. Finally, the configuration of new bifurcations from all the trees with the lowest sum of volumes permanently perfuses the MFU. The detailed description of the aforementioned process in case of the two trees can be find in [7].

The development of a pathological process (*e.g.* tumor) is usually related with changes of functional and structural properties of the tissue, which often entail modifications of vascular structures. These changes are obtained by means of the conversion mechanism introduced in the tissue modeling part. Examples of these connected phenomena will be given in the next section.

### 2.2. *Imaging modality modeling*

The second step of the methodology consists in simulating the physical process underlying the image formation. The methodology is illustrated on CT, but other imaging modalities (Magnetic Resonance Imaging or Ultrasound) fit to this framework. CT has been chosen due to its wide use and the flexibility it offers to control the image conditioning[21]. Variations of the main acquisition parameters (resolution and slice thickness for instance) lead to different appearances of the structures under study. The main steps of CT acquisition modeling based on a simulated organ are depicted in Fig. 5.

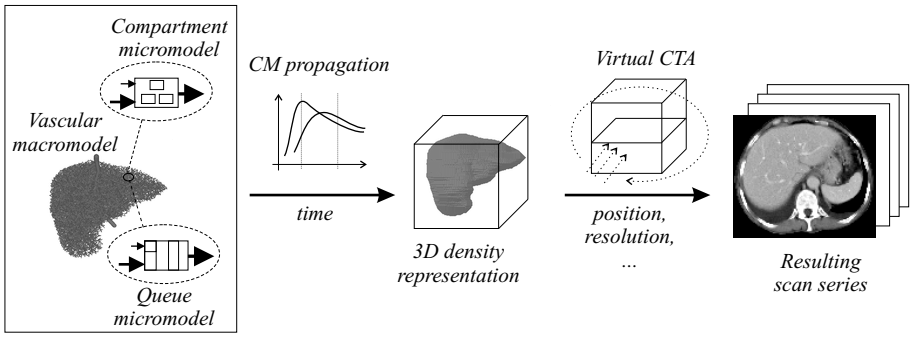


Fig. 5. CT scan-like images of simulated organ are generated from a 3D-density representation created at a given time moment, after injection and propagation of contrast product.

2.2.1. *Contrast material propagation*

A cross-sectional slice of the organ has to be represented in the image. Each voxel of the model volume is associated with a density value so that the resulting 2D image will display the usual CT numbers (the gray level in each pixel of the image is proportional to the CT number of the voxel in the appropriate position).

To create the 3D density representation of the organ, after injection of the contrast material, the concentration evolution has to be known in all vessels and MFUs. In the following description of the contrast product propagation, we consider the most general case of a vascular network made of three trees (like in the liver). In order to simplify the calculation, the concentration is supposed to be constant in each vessel segment and the blood is ideally mixed with the contrast material. In clinical practice the contrast material (CM) is infused intravenously (*e.g.* in an antecubital vein) and after the bolus transfer time it enters the liver, first through the hepatic artery (HA) and then, with a certain delay, through the portal vein (PV). Modeling separately the infusion for the HA and the PV sources, by providing the CM concentration curves at these two entries, gives more flexibility in the simulation of mono or bi-phasic injection with varying conditions (*e.g.* duration, amount of CM) or features specific to a patient (*e.g.* delay between HA and PV).

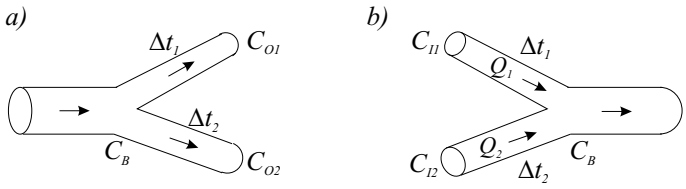


Fig. 6. Propagation of contrast material through bifurcations.

As far as the propagation in the macroscopic network is concerned, the contrast product concentration can be computed at each time $t$, given the concentration in vessels situated upstream (see Fig. 6):

$$C_B(t) = C_{O1}(t + \Delta t_1) = C_{O2}(t + \Delta t_2) \tag{4}$$

The time needed by blood to traverse a vessel can be calculated using its length $l$, radius $r$ and the blood flow $Q$ in it:

$$\triangle t = \frac{\pi r^2 l}{Q} \tag{5}$$

The situation is more complicated when a vessel junction is considered. For the hepatic veins, the concentration at the bifurcation $C_B$ is weighted by the corresponding blood flows:

$$C_B(t) = \frac{Q_1 C_{I1}(t - \Delta t_1) + Q_2 C_{I2}(t - \Delta t_2)}{Q_1 + Q_2}. \tag{6}$$

The propagation of blood and CM through capillaries is a complex process. Two models with different level of simplification can be used to simulate this process. The first one is the queue model originally proposed in Ref. [22]. In a MFU, the volume of capillaries and extracellular space (which is defined as a fraction of the MFU volume) is divided into sections, whose size corresponds to the quantity of blood exchanged during the time interval imposed by the temporal resolution. The concentration of the first section is calculated as weighted concentrations (according to the corresponding blood flows) of the two inputs. The organization of MFU is based on a fixed-size queue (FIFO): at each time, the sections concentrations are shifted. The overall concentration of CM in the MFU is computed as an average concentration of sections. This process is illustrated in Fig. 7. Calculation of the contrast material concentration is depicted at two time moments: arterial phase, when contrast material arrives only through the hepatic artery without contribution of portal vein (left), and portal phase where the contribution of the portal vein is equivalent to the one of the artery (right). For example, on the left top scheme, the CM concentration is 1.0 (maximum possible value) in HA and 0.0 in PV. The resulting value of the first sections concentration is computed by taking into account the respective supplies of HA (1/3 of the total flow) and PV (2/3). The mean concentration of the first section is then 0.33 at time $t_0$. The blood of the first section is then shifted to the next one at time $t_0 + \Delta t$ (left–bottom). In this scheme, the global MFU concentration of CM (0.22) is the mean of the 4 sections (0.33, 0.33, 0.2, 0.0). Right part illustrates the similar process when CM arrives also in PV.

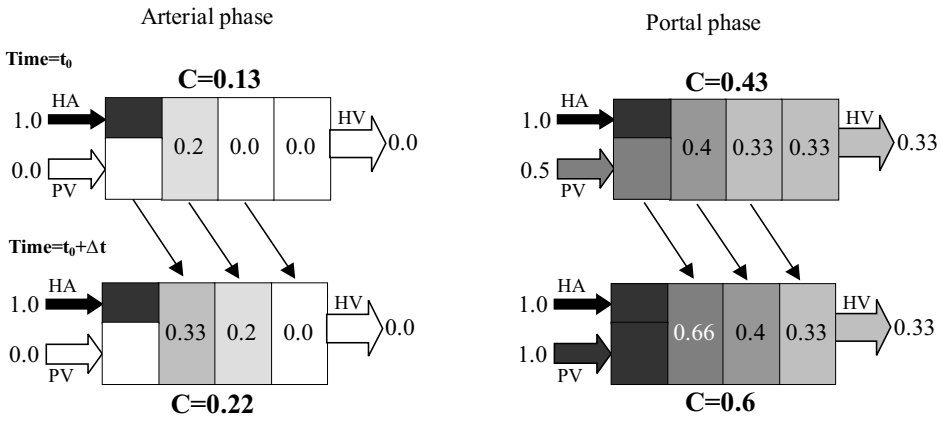


Fig. 7. Queue model of contrast material propagation in MFU

The other approach for the simulation of CM propagation at the microvascular level is based on a compartment model[23]. Recently, this kind of models have been

applied to simulate vessels/tissue exchanges[24,25,26] or to estimate perfusion and capillary permeability[27]. In contrast to some global models, the presented model is local, takes into account the portal circulation, and integrates liquid movements (not only molecules transfer). Moreover, the direct coupling between this microvascular model and the macro-vascular one allow us to generate not only enhancement curves, but also dynamic enhanced images.

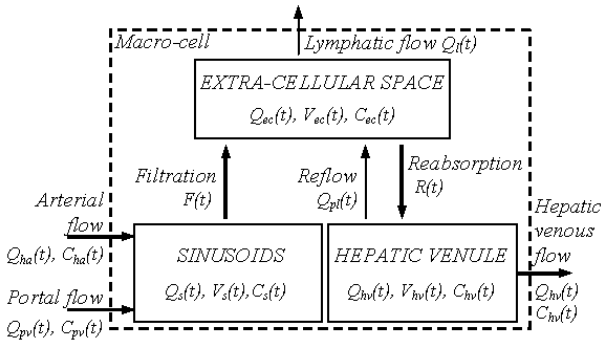


Fig. 8. Three compartment microscopic model used to simulate hepatic transvascular exchanges

The model entries are two blood supplies coming from hepatic arteriole and portal venule. They are characterized by their flows $Q_{ha}(t)$ and $Q_{pv}(t)$ and contrast product concentrations, $C_{ha}(t)$ and $C_{pv}(t)$. The three compartments of the model are depicted in Fig. 8: "sinusoids", "extracellular space" and "hepatic venules". Blood arriving in the sinusoids is mixed with contrast medium at the concentration $C_s(t)$ and goes through the capillary wall into the extracellular space with the flow $F(t)$. Plasma and contrast medium molecules can go out of the extracellular space compartment by two possible ways, due to the hydrostatic and osmotic pressures toward hepatic venules, with the flow $R(t)$ and toward lymphatic capillaries with the flow $Q_l(t)$. In this compartment, the liquid has the concentration $C_{ec}(t)$. Finally, blood leaves MFU by hepatic venule, with the flow $Q_{hv}(t)$. The re-flow $Q_{pl}(t)$ from hepatic venules into extracellular space[28] is also integrated into the model. The contrast material concentration in the third compartment is $C_{hv}(t)$. As the macroscopic vascular model does not currently take into account the lymphatic circulation, the lymphatic flow from the extracellular space ($Q_l(t)$) is artificially connected to the venous circulation ($Q_{hv}(t)$) given only one output: the hepatic venous flow. In order to study concentration variations in the different compartments, exchanges are formalized by the following differential equations:

$$V_s \frac{dC_s(t)}{dt} = C_{ha}(t)Q_{ha}(t) + C_{pv}(t)Q_{pv}(t) - C_s(t)F(t) \tag{7}$$

$$V_{ec} \frac{dC_{ec}(t)}{dt} = C_s(t)F(t) + C_{hv}(t)Q_{pl}(t) - C_{ec}(t)(R(t) + Q_l(t)) \tag{8}$$

$$V_{hv}\frac{dC_{hv}(t)}{dt} = C_{ec}(t)R(t) + C_{hv}(t)(Q_{pl}(t) - Q_{hv}(t)) \quad (9)$$

The compartment volumes are obtained by dividing the volumes corresponding to the whole organ by the number of MFUs. For transvascular flows, general circulation data are used leading to the following relations[24]: $F = Q_{ha} + Q_{pv}$,$R = 0.84F$, $Q_l = 0.21F$ and $Q_{pl} = R + Q_l - F$.

#### 2.2.2. *Virtual scanning*

Here, a full backprojection process[29,30] is applied. The first step consists in creating a 3D map in which each voxel is characterized by a density, taking into account the partial volume effect. The density of a voxel intersecting partially a vessel depends on the volume of the voxel filled by blood and of respective concentrations of contrast material in blood and parenchyma. The volume occupied by blood is computed according to control points regularly distributed into the voxel[31] and situated inside the vessel (Fig. 9).

The number of control points influences the number of vessels effectively represented in the 3D map. The densities of a voxel included in a vessel or only made of parenchyma have been set respectively to the typical values of the blood density and the density of non-injected liver. A gaussian noise has been added to the parenchyma in order to render the spatial variations of microvessels. Using this data volume, the CT scan acquisition is carried out in two steps: X-ray projections are computed, using the Radon function and the filter back-projection method is used to reconstruct the image. In order to take into account the thickness of the beam, not only the voxel intersected by a ray has to be considered but also its neighbors, that have also been touched by the beam. An interpolation method is applied to compute the resulting attenuation (the contribution of a neighbor with density $\alpha$ and whose center is situated at a distance $D$ of the point is set to $\alpha(1 - D)$).

## 3. Applications

In this section, applications of the model-based approach are described. First, simulation results of two vital abdominal organs (namely liver and kidneys) are pre-

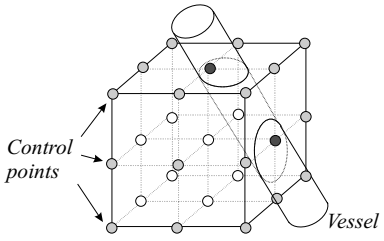


Fig. 9. The density assigned to a voxel depends on the volume of the voxel inside a vessel. To compute it, control points distributed in the voxel are used.

sented in normal conditions. Then pathological processes are induced and dynamic CT images of these processes are generated during the contrast material propagation. Finally series of simulated images are analyzed by means of texture analysis methods.

### 3.1. *Simulation of growth and pathological modifications*

#### 3.1.1. *Kidney growth in normal conditions*

The 3D shape used to simulate the kidney in different steps of its growth is obtained by a manual segmentation of CT slices followed by an interpolation of the segmented 2D Regions Of Interest, which finally provides a binary 3D representation of the organ (Fig. 10).

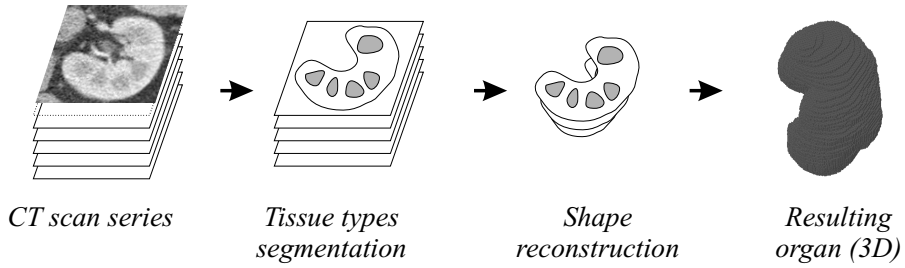


Fig. 10. Generation of the binary shape used as a 3D constraint during simulation of the kidney growth.

Geometrical and hemodynamical parameters used during the simulation of the kidney growth are summarized in Table 1. They deal with the organ (size, number of MFUs) and with the vascular network (blood pressure and flow).

Table 1. Main parameters used for the kidney simulation

| Model parameter | Arterial tree | Venous tree |
|---|---|---|
| Blood pressure at the input ($mmHg$) | 95 | 10 |
| Blood pressure at the output ($mmHg$) | 15 | 5 |
| Blood flow (ml/min) | 500 | |
| Number of MFU-s in the adult organ | ∼3200 | |
| Change of the organ's size (initial→adult) ($cm^3$) | 10→400 | |

Results of simulation are displayed in Fig. 11. The arterial and the venous trees are represented at the very beginning of the growth, after few cycles and at the end.

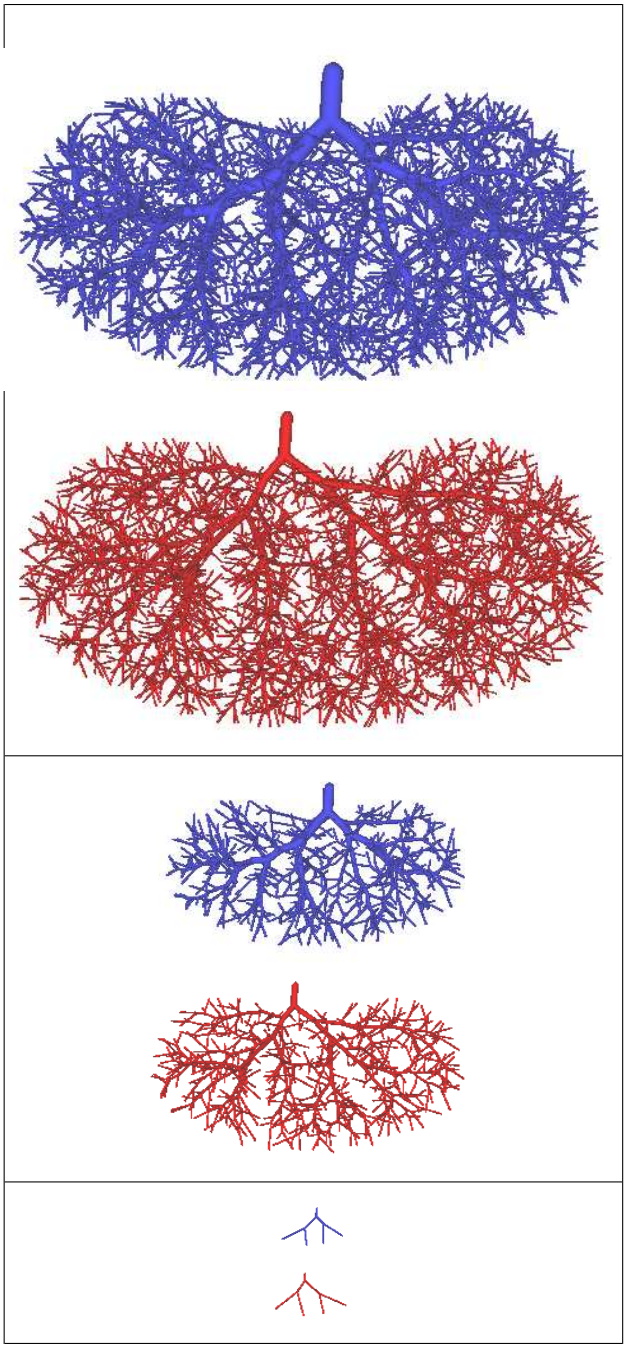

Fig. 11. Simulation results of kidney vascular system development (in each panel arterial tree on the left and venous tree on the right)

3.1.2. *Pathological modifications in the liver*

The model was applied to simulate the growth of liver vascular structures in two pathological cases (hyper- and hypovascular tumor). The hepatic vascular system is very specific because of its three trees. All of them can be simultaneously simulated by the model, taking into account their geometric and hemodynamic relations. The hepatic veins can be seen as the only output (it carries blood out of the liver, to the vena cava and then to the heart) and are here coupled either with the hepatic arteries or with the portal veins. The main parameters used to illustrate the model behavior are defined in Table 2. The 3D bounding shape of the liver has been reconstructed from CT-scan images (Siemens Somaton, 120 slices with 1 mm thickness) after interactive delineation with the process described in Fig. 10. The model was initialized with three trees consisting only of 7 vessels each. The geometry of this initial network was chosen based on anatomical data. The structure of the largest vessels is kept the same for the HA or for the PV because they are effectively very similar in their main branches.

Table 2. Main parameters used in the simulation of liver.

| Model parameter | Hepatic artery | Portal vein | Hepatic vein |
|---|---|---|---|
| Blood pressure at the input ($mmHg$) | 95 | 25 | 12 |
| Blood pressure at the output ($mmHg$) | 20 | 15 | 5 |
| Wall thickness ratio (fraction of radius) | 0.2 | 0.1 | 0.1 |
| Blood flow (ml/min) | 400 | 1100 | 1500 |
| Number of MFU-s in the adult organ | | ∼12000 | |
| Change of the organ's size (initial→adult) ($cm^3$) | | 75→1500 | |

The 3D vascular model can be used to simulate hypervascular lesions like, for example, the Hepatocellular Carcinoma (HCC), which represents the most common hypervascular hepatic malignant tumor. The main differences between the normal vascularization and the HCCs one is that this kind of tumor has only an arterial blood supply and does not receive portal venous blood flow, whereas normal hepatic tissue is perfused by the three trees. A second class of MFU is used to simulate a focal lesion in normal parenchyma. Few abnormal MFU are introduced among normal ones in a bounded area of the organ. Then, these tumoral MFUs co-exist with the healthy ones and evolve with them in a succession of regeneration events (mitosis/necrosis). Some parameters associated to this second class of MFUs are different from the normal ones: probability of mitosis, maximum local density and blood flow are increased in the pathological case. Figure 12 shows tumoral MFUs among normal ones. Moreover, when a new tumoral MFU appears, only a hepatic arteriole and a hepatic venule sprout from the existing network, but no portal venule.

The vascular modifications implied by HCC can be seen in Fig. 13, where the three hepatic trees corresponding to healthy liver (left column) and liver with HCC (middle column) are displayed.

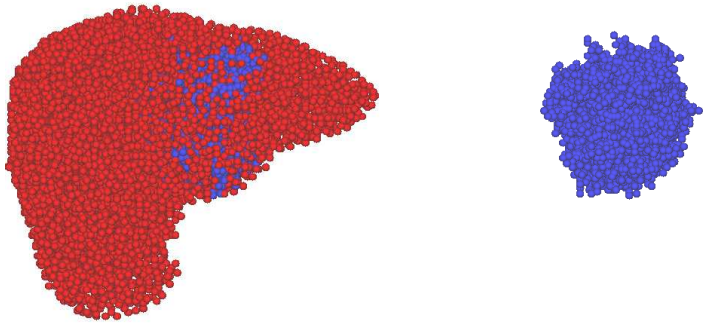

Fig. 12. Illustration of normal and tumoral MFUs in liver

In the same way, a hypovascular tumor can be simulated by introducing a new class of MFUs with different parameters. This time the necrosis probability is increased, which leads to a progressive disappearance of MFUs and creation of a hypovascularized region in the liver (Fig. 13, right column).

### 3.2. *Virtual CT scanning*

In this section, we illustrate the coupling between the model of liver and the model of CT modality. These two models are used to generate dynamic CT images of the liver, where local pathological changes can be tracked during the CM propagation.

#### 3.2.1. *Contrast product propagation in liver*

Hepatic hemodynamic interactions are very complex because of the dual blood supply of the liver: 20-25% of the blood comes directly from the aorta, through the hepatic artery and 75-80% from the mesentery through the portal vein. At the entry of the hepatic capillaries (sinusoids) the two flows mix.

In clinical routine, spiral CT scanning after injection of contrast medium provides high quality images of the liver and the capability to fully explore the organ during arterial and portal phases. It improves the detection and the characterization of hepatic tumors by amplifying the difference in attenuation between the tumor and the normal parenchyma[32,33]. Distinction of the two main phases of the liver enhancement is of great clinical interest: it allows determining the optimal temporal windows for the liver exploration and for a maximal conspicuity of tumors. For example, hypervascular hepatic lesions are better detectable during the pure arterial phase when the contribution of the portal blood supply is not preponderant yet. But the duration of this phase is difficult to estimate[34]. This is mainly due to the variations of the hepatic enhancement with a large number of parameters (type and quantity of contrast material, injection flow and duration, monophasic or biphasic

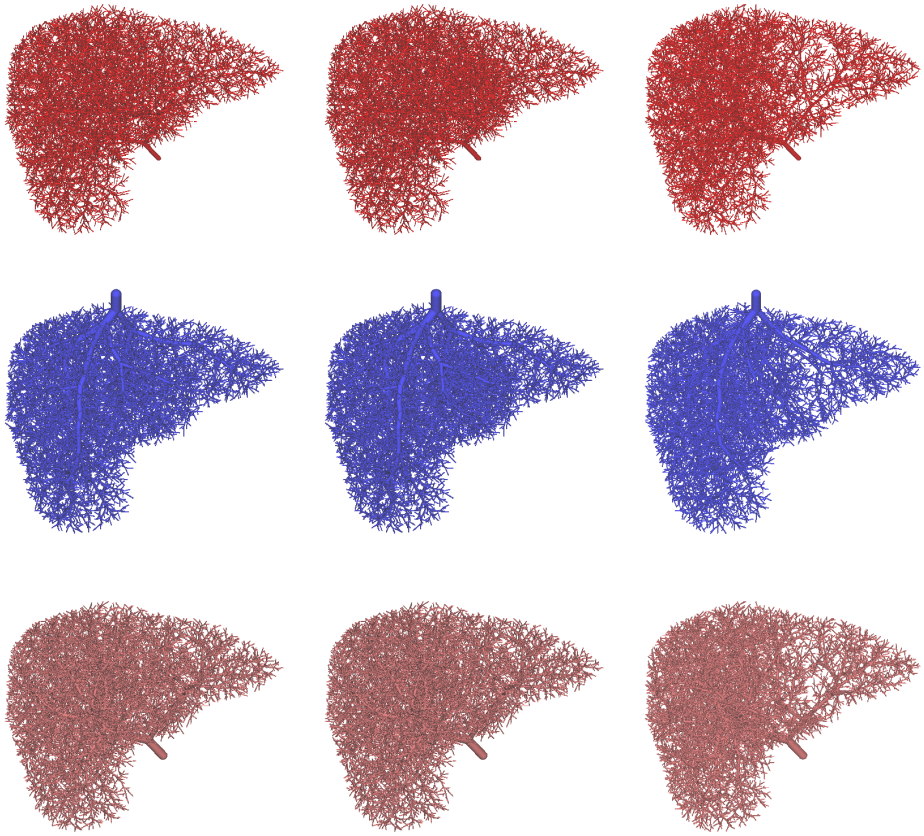

Fig. 13. Hepatic vascular network simulated in three cases: normal (left), hypervascularization (middle), hypovascularization (right). Each tree is presented separately to enable a better visualization, but they are physically connected.

injection) or the tumor types[35].

Many clinical studies have been performed during the last 15 years, in order to understand the influence of all these features. For instance, in Ref 36, it is shown on a group of 109 patients that the risk of missing a tumor decreases with a double phase acquisition, compared to a simple one. In Ref. 37, the influence of the quantity of contrast product, and the injection flow is evaluated on 25 patients, concluding that augmenting the CM flow results in an acceleration of the hepatic enhancement.

Dodd and Baron[38] underline the lack of standardization of clinical studies, whose results are difficult to compare. Indeed, in some of these studies, extrinsic parameters (depending of the CM administration and the image acquisition protocol, number of slices, level of slices) are often heuristically chosen with an important part of randomness, and significant intrinsic parameters can be ignored. The necessity to

control these parameters is still amplified by the fast advances that intervene in the imaging technology as well as in the field of contrast materials, limiting the usefulness of clinical studies.

Few models of the liver enhancement have been proposed so far. Bae *et al.*[25] applied their compartmental model of the human cardiovascular system to simulate enhancement curves corresponding to three groups of patients with varying height and weight. The model presented in Ref. 26 is also interesting to quantify the hepatic perfusion and to extract anatomical and functional properties from a CT acquisition. Work of Kim *et al.*[39] is based on a compartmental model of the liver, including a tumor. This model is used to simulate enhancement curves and to predict the optimal injection protocol. All these models are useful to simulate curves corresponding to the whole liver but cannot be used to synthesize images or local vascular modifications. Thus, we applied the physiological model of the liver coupled with the model of CT images in order to create hepatic dynamic CT scans.

In Fig. 14, the arterial and portal phases of contrast product propagation are presented (enhanced 3D vascular trees and a corresponding CT slice) in the case of a hypervascular tumor.

During the arterial phase the lesion can be detected easily: it appears more intense than normal surrounding parenchyma. During the portal phase the lesion becomes slightly hypodense when compared to normal tissue. This enhancement is in agreement with what is observed during the classical radiological examination, realized for this kind of disease. During the first early acquisition phase (around 20-30 s after contrast infusion) HCC receives highly concentrated CM coming from the HA, while the liver parenchyma is less enhanced because receiving less CM (PV does not contain CM yet), which leads to a high lesion conspicuity. Then, in the other phase, the normal parenchyma is strongly enhanced due to the important flow of CM arriving through the PV (representing about 80% of the total flow) whereas the tumor CM supply (only arterial) diminishes. It leads to the inversion of the enhancement and to the decrease of conspicuity.

The same kind of simulation has been performed in the case of hypovascular tumor. Figure 15 shows arterial and portal phases of contrast product propagation (enhanced 3D vascular trees and corresponding CT slices) for this second kind of disease.

The hypovascular region is visible during both, the arterial and the portal phase, because the contrast product concentration is always lower in this region than in normal parenchyma. So, the tumor conspicuity essentially depends on the contrast concentration in normal parenchyma. It is the reason why it is more important during the portal phase (given the proportion between arterial and portal flows).

### 3.3. *Texture analysis of hepatic CT*

Semi-automatic and objective tissue characterization still remains an open problem for many types of imaging modalities and organs. Texture analysis is useful to

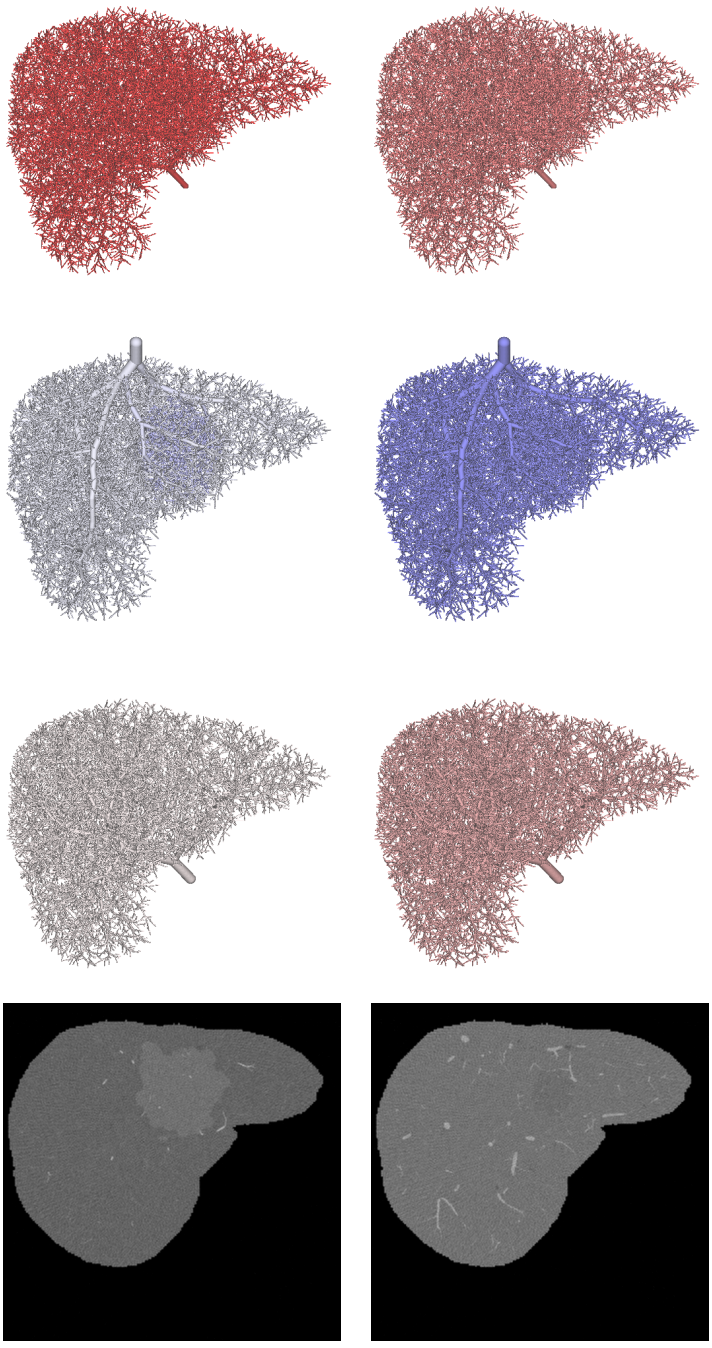

Fig. 14. Enhancement of a hypervascular lesion in 3D (HA, PV, HV) with the corresponding CT acquisition during the arterial (left column) and portal phases (right column). The scan is generated at the tumor level. The CT slice characteristics are: 512x512 matrix, 8-bit gray levels, 4 mm thickness.

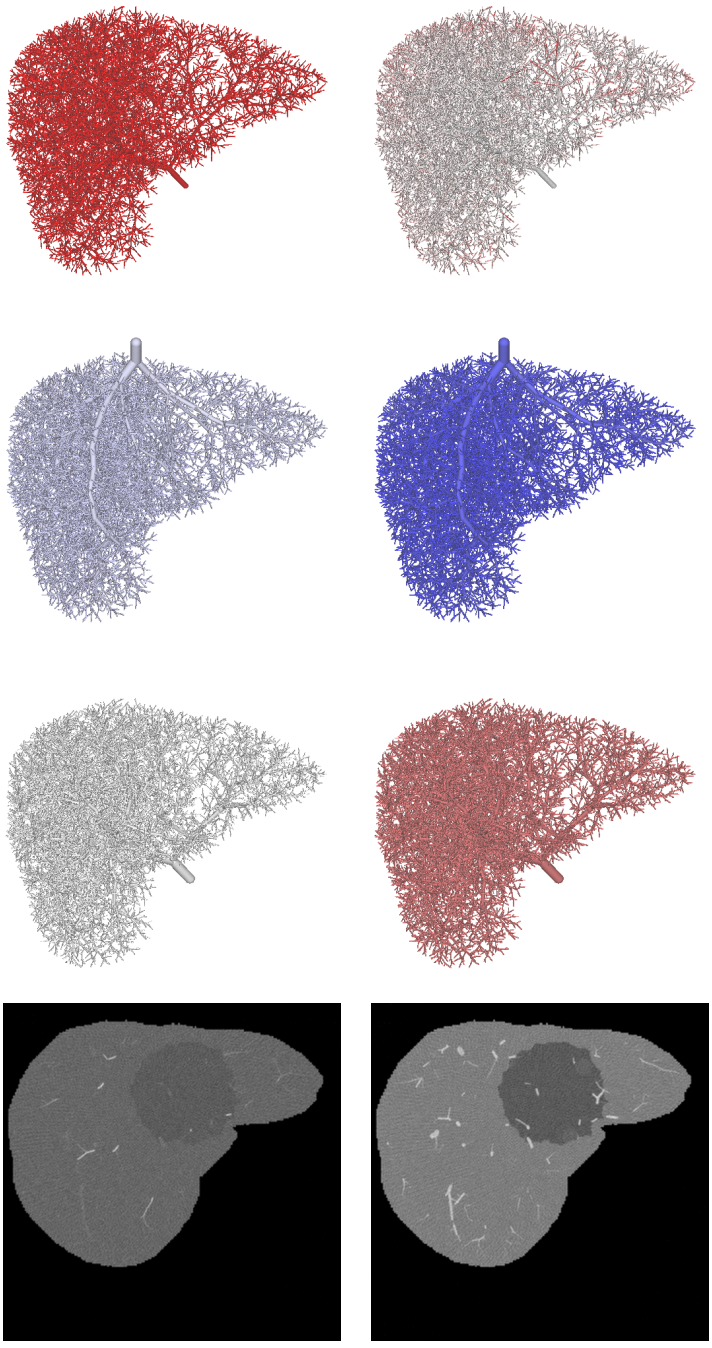

Fig. 15. Enhancement of a hypovascular lesion in 3D (HA, PV, HV) with the corresponding CT acquisition during the arterial (left column) and portal phases (right column). The scan is generated at the tumor level. The CT slice characteristics are: 512x512 matrix, 8-bit gray levels, 4 mm thickness.

describe homogeneous areas of medical images. It consists in extracting a set of parameters to characterize Regions Of Interest (ROI) defined in the organs under study.

These features are generally derived from simple (e.g. first-order and gradient-based statistics) or more sophisticated (for example based on co-occurrence or run-length matrices) statistical properties of the image[40]. Another possibility encompasses model-based approaches (e.g. fractals[41] and Markov fields[42]), transform methods (e.g. based on Fourier, Gabor[43] or wavelet transformations[44]) and mathematical morphology operations[45].

Texture analysis is known to be very sensitive for the discrimination of pathologies[46]. It was successfully applied to a broad range of imaging modalities and diagnostic problems such as: dystrophy of skeletal muscle (MRI)[47], breast nodules (ultrasound B-scan)[48], botulism on trabecular bone (X-ray radiograms)[49], solitary pulmonary nodules (CT)[50], coronary plaques (intravascular ultrasound)[51]. Even if all these works lead to potentially interesting results, common difficulties have been raised.

The number of potential textural features is high and it is generally not easy to choose the most meaningful ones given the organ, its pathology and the imaging modality. This task is especially difficult for medical doctors without a great experience in texture analysis. The straightforward mapping of the extracted parameters to image characteristics used by the radiologists during their visual analysis is not always possible, what may explain why these automatic methods are not extensively used in clinical routine. Another difficulty lies in the lack of standardization of methods used to acquire and analyze images, which makes difficult any reliable comparison of the results obtained in various centers. The need to define appropriate protocols is unquestionable, but achieving the consensus is very difficult, especially because it depends on the acquisition equipment. This situation emphasizes the difficulties to control and reduce the variability of the features as reported in the literature.

Computational modeling of the texture formation process can be useful to face aforementioned problems and to better understand the relation between observed image data and underlying tissue properties. The coupled models presented in the previous section allow us to control the full process of image formation. Even if modeling remains only an approximation of reality, it offers the possibility to scan repeatedly the same organ with various acquisition conditions, and then to study the influence of acquisition parameters on texture[52]. In this paragraph, these images are presented, and the evolution of certain textural features is illustrated, at different times, and for the two pathological cases already mentioned (hyper- and hypovascular tumor)[53]. We don't give here the definition of textural features that are used. They can be found in literature (e.g. in Ref. 40).

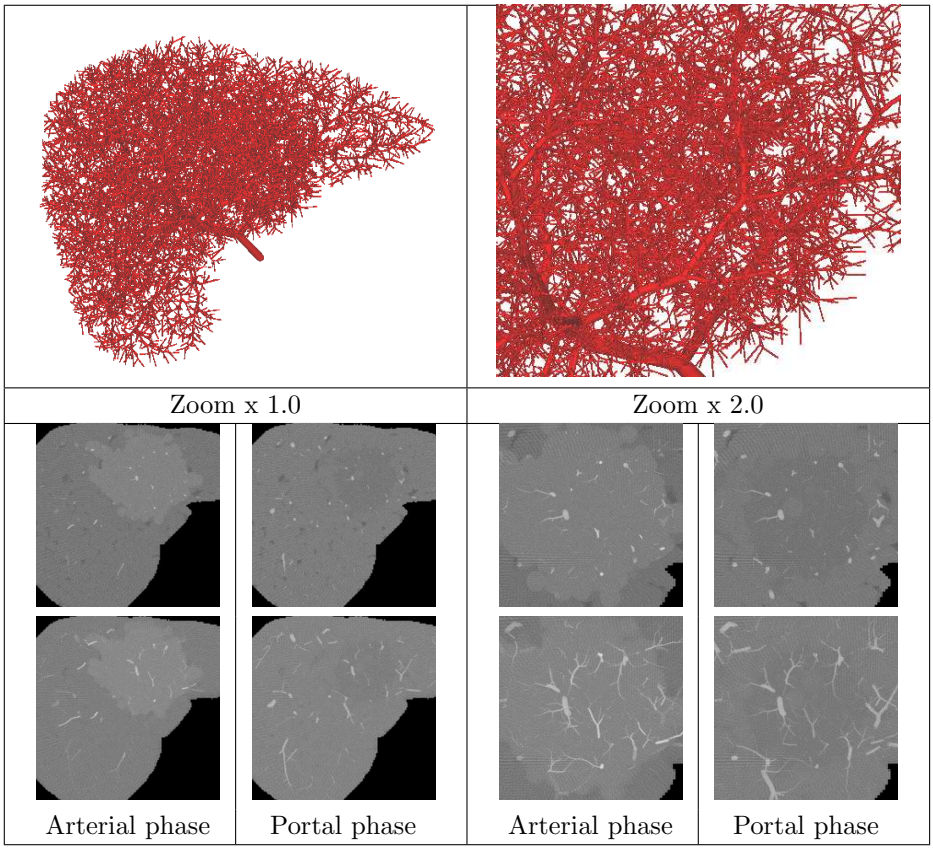


Fig. 16. Arterial tree with the hypervascularized region and the corresponding CT scans (at arterial and portal phase with varied spatial resolution and slice thicknesses).

### 3.3.1. *Hypervascular lesion*

Figure 16 shows the simulation results of the hepatic arterial tree perfusing a liver with an hypervascular lesion. The 3D vascular tree is presented with two different resolutions (Zoom $\times$ 1, Zoom $\times$ 2). In the same figure eight simulated CT scans are shown, four at each resolution. For each resolution, two images correspond to a 2 mm slice thickness and two have been synthesized with a 8 mm thickness. Among the two images with a given thickness, one is simulated during the clinical "arterial phase" of acquisition, and the other during the "portal phase".

A visual inspection of the simulated images already shows significant differences among scans acquired with different parameters (spatial resolution, slice thickness and time). On the 2 mm thick slices, vessels resemble dots, whereas on thicker ones, segments and bifurcations can be easily distinguished. In addition, when the spatial resolution is increased (by zooming) the number of visible details is augmented. It can be expected that some textural features will vary with changes of acquisition

conditions. In order to study their evolution with these parameters, the calculation of features is conducted for 8 slice thicknesses (1 to 8 mm), 6 resolutions (from x1.0 to x2.0) and 2 time instants (corresponding roughly to arterial and portal phases), what gives almost 100 combinations.

Circular, large (50 pixels radius) ROI-s are placed at the center of lesions and in the normal tissue. Textural features obtained by classical statistical methods (first order, gradient based, co-occurrence and run-length matrix based) are computed. The features corresponding to four angles (0, 45, 90 and 135) (*e.g.* all derived from run-length matrix) were averaged.

In Fig. 17, the evolution of three features according to the slice thickness and the zoom is depicted at 2 acquisition times. The first one is the well-known "average of gray levels". Even if it gives information only on the image intensity, and not exactly on the spatial repartition of the gray levels, it is important to mention it in this particular case: it is often used by radiologists to detect and characterize a tumor. The second one, the "gray level distribution", is derived from the run-length matrix. The third one is "correlation" calculated from the co-occurrence matrices.

On each graph, feature values corresponding to healthy tissue are compared with that of the lesion. In case of a hypervascular tumor, the average gray level of the lesion is higher in the full range of tested resolutions during the arterial phase. The completely reversed situation can be observed during the portal phase. Considering the gray level distribution, it can be noticed, that the two surfaces, describing the evolution of this feature, intersect in a similar way at both phases. As far as the third parameter is concerned, it seems to be useful only during the portal phase. In this case, influence of the spatial resolution is predominant (discrimination between normal and pathology is correct for zooming superior to 1.6 for all thicknesses).

#### 3.3.2. *Hypovascular lesion*

The same kind of simulations have been performed in the case of a hypovascular lesion. Results are presented in Fig. 18, in the same manner as in the hypervascular case.

Corresponding textural features are represented in Fig. 19. The representation of the "average of gray levels" confirms the tumor hypodensity at the two phases, with a slightly greater difference at the portal phase, whatever the resolution and the slice thickness. The second parameter seems more efficient during the portal phase, and in both cases the best discrimination is obtained for extreme values of resolution and thickness. Concerning the third parameter, it doesn't show any interest in portal phase, but could be useful in arterial phase if the resolution and thickness are sufficient.

These results confirm that different acquisition conditions of CT scanning influence strongly the texture observed on images. They also point out that textural features can potentially be used for discrimination purposes in clinical examinations, but only when the same (or at least similar) protocols are used.

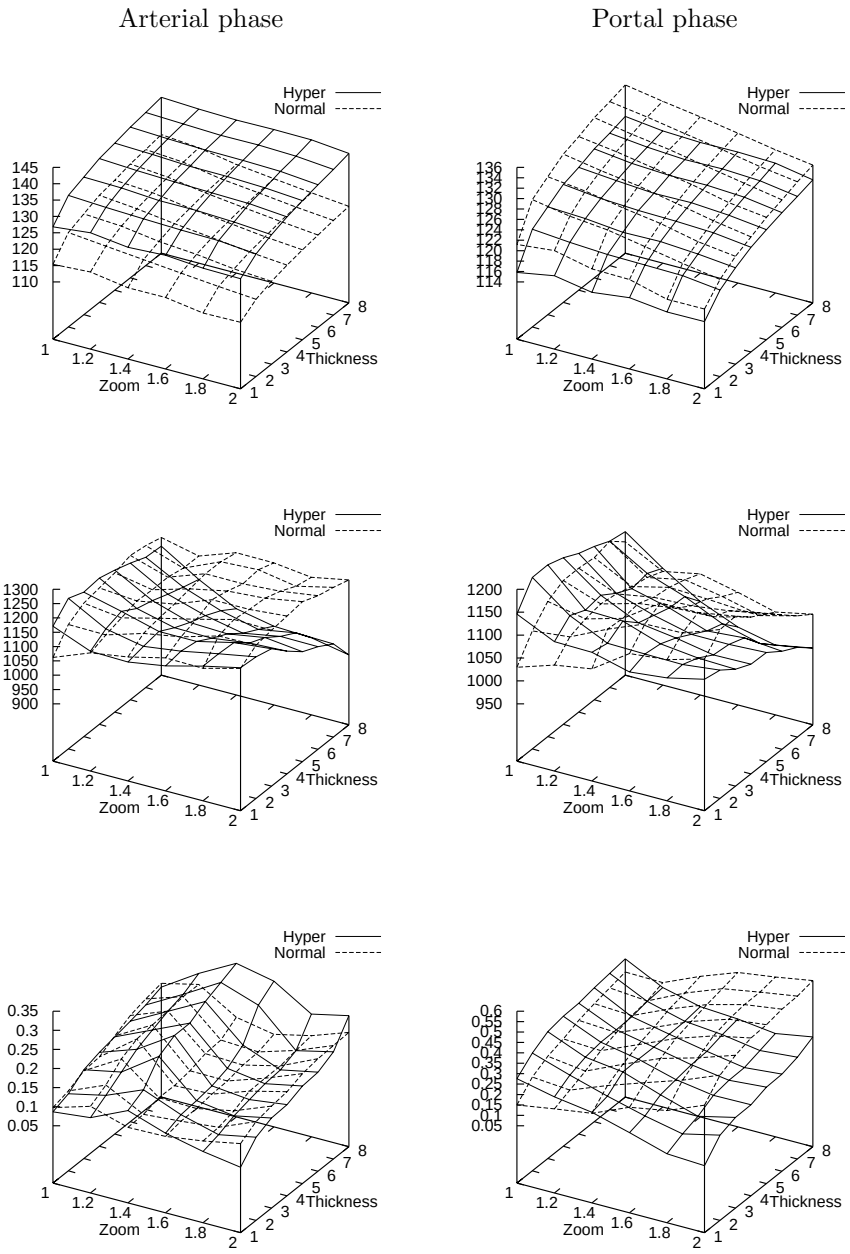


Fig. 17. Evolution of three textural features (average of gray levels, gray levels distribution, and correlation) with slice thickness and resolution, at arterial (left column) and portal (right column) times. On each graph, feature values calculated inside the hypervascular lesion are confronted with those corresponding to normal tissue.

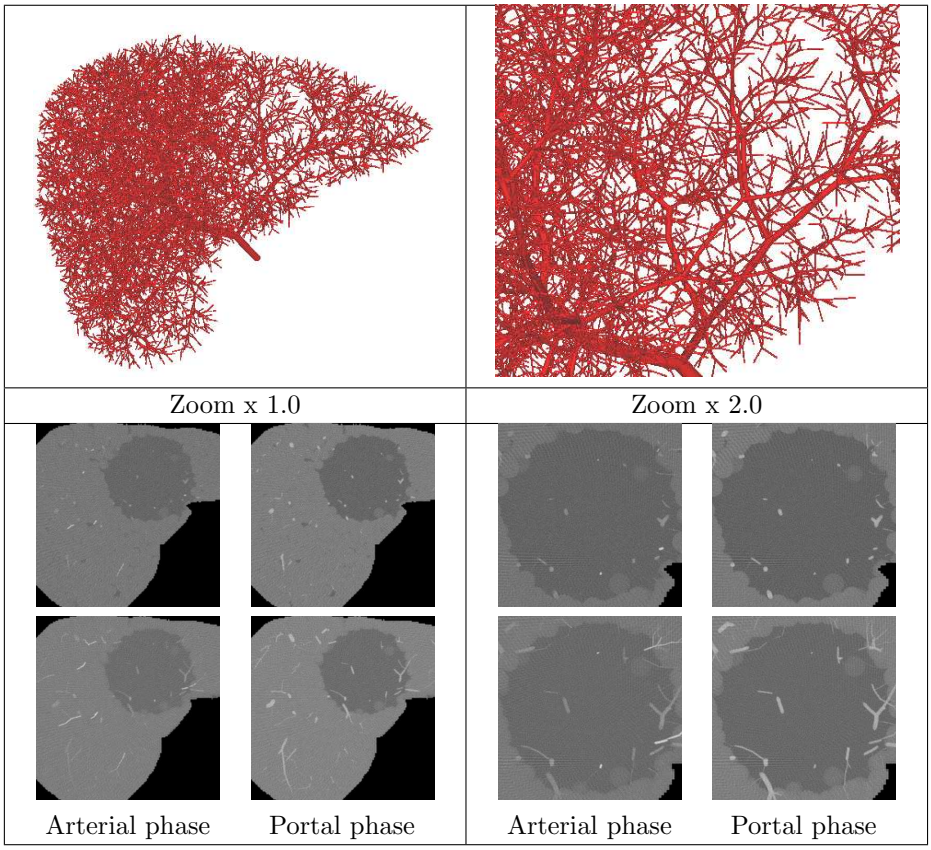


Fig. 18. Arterial tree with the hypovascularized region and the corresponding CT scans (at arterial and portal phase with varied spatial resolution and slice thicknesses)

In the preceding experiments, the features were calculated from simulated CT images generated only at two time moments, corresponding to standard clinical acquisition times (arterial and portal phase). However, tissue characterization can also be ameliorated by considering the evolution of characteristics during all the contrast medium propagation through the organ. Dynamic CT scans have been synthesized, every second, during contrast propagation through the liver, using the compartment model presented in the preceding section. Injection profiles we used have been taken from Ref. 39, corresponding to the evolution of hepatic artery and portal vein concentrations with time during three minutes.

Hepatic enhancement was measured in these simulated images, in normal tissue and in hypervascular tumor. Relative enhancement (compared to the simulated CT scan before injection) over time is displayed in Fig. 20. These curves are very close to real liver enhancement (curves can be found in Ref. 39). They show a rapid concentration rise in the tumor (supplied only by HA) followed by a similar increase

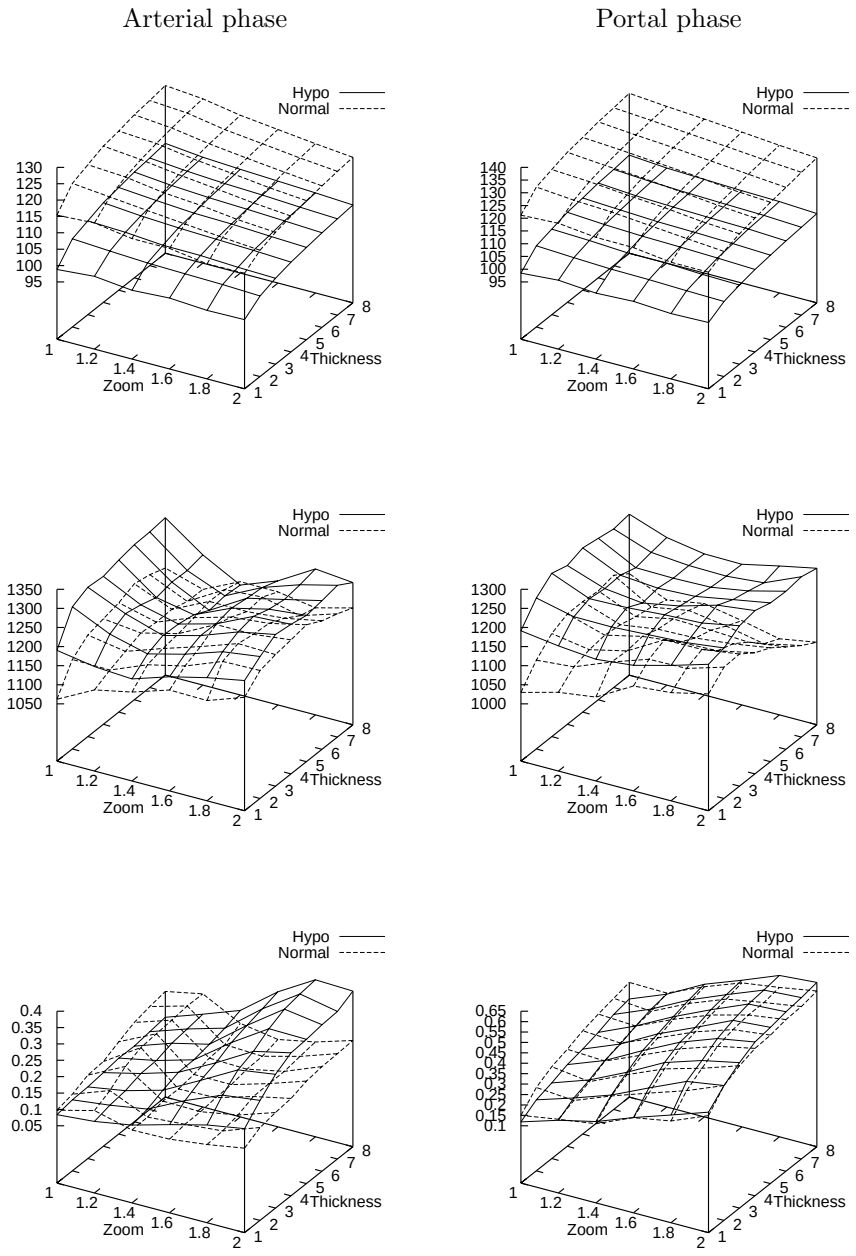


Fig. 19. Evolution of three textural features (average of gray levels, gray levels distribution, and correlation) with slice thickness and resolution, at arterial (left column) and portal (right column) times. On each graph, feature values calculated inside the hypovascular lesion are confronted with those corresponding to normal tissue.

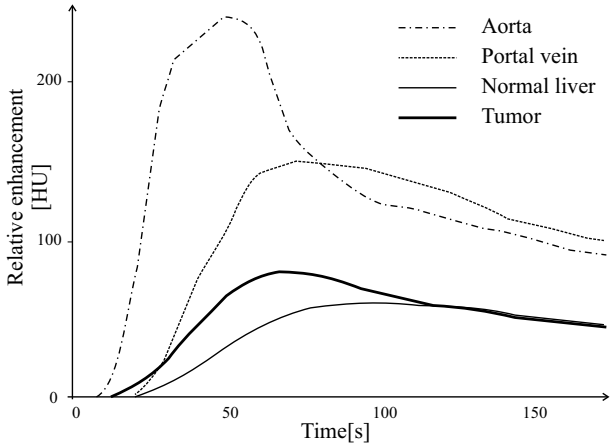


Fig. 20. Enhancement curves resulting from simulated CT scans of the liver. Enhancement in normal parenchyma and the lesion are represented in solid lines. Dotted lines correspond to injection profiles in the hepatic artery and the portal vein.

in normal tissue (supplied by both HA and PV), and a slower decrease in both of these vessels, tending to an equilibrium between normal and tumoral tissues.

These experiments show that combining the two models, one for the macro-vascular trees, and the other for micro-vessels, provides a realistic model of dynamic hepatic enhancement in CT. The same kind of dynamic measures can be made for textural features.

## 4. Conclusion

In this chapter we propose a general framework for medical image analysis based on modeling. The framework is composed of a model of organ coupled with a model of image acquisition. It is exemplified on the particular case of *i)* parenchymous organs with a highly developed vascular network, and *ii)* Computed Tomography acquisition.

The organ and its vascular network are simulated by a knowledge based model, including physiological rules (pressure, blood flow and vascular density) and morphological boundary constraints. The organ growth is reproduced, during which new vessels progressively appear to answer to increasing blood needs. The model of image acquisition is based on the physical process of Computed Tomography. It is used to synthesize timed-stamped series of images with varying parameters (e.g. spatial resolution) after injection of a contrast material through the vessel network and the parenchyma. At the microscopic level, two models are proposed to simulate the exchanges between blood vessels and tissue: a simple one, based on a queue principle (First In, First Out), and a more precise one resorting to compartmental theory.

Two main applications are presented, concerning vital organs: the kidney and the liver. In the normal case, the vascular networks of these two organs are quite different: the renal vascularization is made of two trees, while the hepatic vascularization is very particular due to the presence of three connected trees. Vascular modifications related to pathology are also illustrated by modeling hepatic hypervascular (and hypovascular) tumors. CT scans are generated in these pathological conditions with two acquisition delays after contrast infusion: early arterial phase and later portal phase. The coupled models have been used to simulate the enhancement of a hypervascular tumor (e.g. Hepatocellular Carcinoma) at different acquisition times. These simulated images are in agreement with real acquisitions, showing a maximum conspicuity of the lesion during the arterial phase, with an hyperdensity compared to normal parenchyma and a slightly inverted contrast, almost obscuring the lesion during the portal venous phase. The final step of this model based approach deals with tissue characterization. Classical methods of texture analysis (co-occurrence, gradients and run-length) have been applied on images representing healthy and tumoral liver with various acquisition parameters.

These experiments show how this kind of physiological model coupled with a physical model of acquisition can help *i)* to better understand the complex interactions at the origin of dynamic enhancement of organs in medical images and *ii)* to relate generally abstract textural features to more explicit anatomic or functional properties.

Future work will deal with the evaluation of the influence of acquisition conditions on the efficiency of textural features to characterize pathological tissues. Studying the influence of the injection protocols (changing the injection time profiles) on images and on the typical time measurements (for instance, duration of the hepatic arterial phase) will also be possible in this framework. This model-based approach should be useful in the optimization of injection protocols and acquisition times, for *in vivo* examination. Moreover, other organs and other diseases can be considered in this modeling approach, in order to appreciate how vascular failure occur and what can be their repercussion on the organ anatomy and function. Models of other acquisition modalities can also be developed, like for instance Ultrasound or Magnetic Resonance Imaging.

*Acknowledgments*

The authors are grateful to Prof. Jean-Louis Coatrieux and Prof. Leon Bobrowski for their support and for inspiring discussions. They also thank Dr. Yan Rolland for his clinical contribution. The works presented in this chapter were supported by the grant W/WI/5/05 from Bialystok Technical University.

## References

1. B. Zeigler, H. Praehofer and T.G. Kim, *Theory of Modeling and Simulation*, second edition, Academic Press (1999).

2. J. Mattes, J. Fieres, J. Beaudoin, D. Gerlich, J. Ellenberg and R. Eils, *Lect. Notes Comput. Sc.* 2208, 1323 (2001).
3. J. Demongeot, J. Bézy-Wendling, J. Mattes, P.Haigron, N. Glade and J.L. Coatriuex, P. IEEE 91(10), 1723 (2003).
4. J.L. Coatrieux, *Int. Cong. on Computational Bioengineering, September 24-26, Zaragoza, Spain*, (2003).
5. E. Carson and C. Cobelli, *Modelling Methodology for Physiology and Medicine*, Academic Press (2001).
6. F.C. Hoppensteadt and C.S. Peskin, *Modeling and Simulation in Medicine and Life Sciences*, second edition, Springer Verlag (2001).
7. M. Krętowski, Y. Rolland, J. Bézy-Wendling and J.L. Coatrieux, *IEEE T. Med. Imaging* 22(2), 248 (2003).
8. F. Wendling, F. Bartolomei, J.J. Bellanger and P. Chauvel, *Eur. J. Neurosci.* 15(9), 1499 (2002).
9. O. Cinquin and J. Demongeot, *C. R. Biol.* 325(11), 1085 (2002)
10. R.J. Goss, in *The Strategy of Growth*, Eds. H. Teir and T. Rytomaa, (Academic Press, 1967).
11. J. Bézy-Wendling and A. Bruno, *J. Biol. Syst.* 7(1), 11 (1999).
12. M. Zamir, *J. Gen. Physiol.* 118, 267 (2001).
13. M.E. Gottlieb, *Proc. Int. Conf. of the IEEE EMBS* 12(3), 1386 (1990).
14. F. Nekka, S. Kyriacos, C. Kerrigan and L. Cartilier, *B. Math. Biol.* 58(3), 409 (1996).
15. W. Schreiner and P.F. Buxbaum, *IEEE T. Biomed. Eng.* 40(5),482 (1993).
16. Y. Rolland, J. Bézy-Wendling, R. Duvauferrier and A. Bruno, *Invest. Radiol.* 34(3), 171 (1999).
17. R. Karch, F. Neumann, M. Neumann and W. Schreiner *Comput. Biol. Med.* 29, 19 (1999).
18. M. Zamir and H. Chee, *Can. J. Physiol. Pharm.* 64, 661 (1986).
19. D.L. Cohn, *B. Math. Biophys.* 16, 59 (1954).
20. M. Krętowski, Y. Rolland, J. Bézy-Wendling and J.L. Coatrieux, *Comput. Meth. Prog. Bio.* 70(2), 129 (2003).
21. Y. Rolland, J. Bézy-Wendling, R. Duvauferrier and J.L. Coatrieux, *Invest. Radiol.* 34(3), 181 (1999).
22. J. Bézy-Wendling, M. Krętowski and Y. Rolland, *Comput. Biol. Med.*33(1), 77 (2003).
23. J. Bézy-Wendling, M. Krętowski and P. Coupe *Proc. of ISBI'04*, 444 (2004).
24. J.L. Bert and K.L. Pinder, *Simulation* 39, 89 (1982).
25. T. Bae, P. Heiken, and A. Brink, *Radiology* 207, 647 (1998).
26. R. Materne, B.E. Van Beers, A.M. Smith, I. Leconte, J. Jamart, J.P. Dehoux, A. Keyeux and Y. Horsmans, *Clin. Sci.* 99, 517 (2000).
27. G. Brix, M.L. Bahner, U. Hoffmann, A. Horvath and W. Schreiber, *Radiology* 210, 269 (1999).
28. C. Chapple, B.D. Bowen, R.K. Reed, S.L. Xie and J.L. Bert, *Comput. Meth. Prog. Bio.* 41, 33 (1993).
29. G.T. Herman, *Image Reconstruction from Projections, the Fundamentals of Computerized Tomography*, Academic Press (1980).
30. A.C. Kak and M. Slaney, *Principles of Computerized Tomographic Imaging*, IEEE Press (1988).
31. J. Bézy-Wendling, M. Krętowski, Y. Rolland and W. Le Bidon, *IEEE T. Biomed. Eng.*, 48 (1), 120, (2001).
32. D. Bluemke and E. Fishman, *Am. J. Radiol.* 160, 787 (1993).
33. R.L. Baron, Am. J. Radiol. 163, 323 (1994).

34. M.G. Frederick, B.L. McElaney, A. Singer, K.S. Park, E.K. Paulson, S.G. McGee and R.C. Nelson, *Am. J. Radiol.* 166, 1305 (1996).
35. M.M. Walkey, *Radiology* 181, 17 (1991).
36. V. Bonaldi, P. Bret, C. Reinhold and M. Atri, *Radiology* 197, 357 (1995).
37. W.C. Small, R.C. Nelson, M.E. Bernardino and L.T. Brummer, *Am. J. Radiol.* 163, 87 (1994).
38. G.D. Dodd and R. Baron, *Am. J. Radiol.* 160, 643 (1993).
39. S. Kim, J.H. Kim, J.K. Han, K.H. Lee and B.G. Min, *Comput. Med. Imag. Grap.* 24, 317 (2000).
40. R.M. Haralick, *P. IEEE* 67(5), 786 (1979).
41. C.C. Chen, J.S. Daponte and M.D. Fox, *IEEE T. Med. Imaging* 8, 133 (1989).
42. G.R. Cross and A.K. Jain, *IEEE T. Pattern Anal.* 5(1), 25 (1985).
43. D.A. Clausi and M.E. Jernigan, *Pattern Recogn.* 33, 1835 (2000).
44. S.G. Mallat, *IEEE T. Pattern Anal.* 11(7), 674 (1991).
45. R. Haralick, S.R. Sternberg and X. Zhuang *IEEE T. Pattern Anal.* 9(4), 532 (1989).
46. A. Bruno, R. Collorec, J. Bézy-Wendling, P. Reuz and Y. Rolland, in *Contemporary Perspectives in Three-dimensional Biomedical Imaging*, Eds. C. Roux and J.L. Coatrieux), (IOS Press, 1997), p. 133.
47. S. Herlidou, Y. Rolland, J.Y. Bansard, E. Le Ruleur and J.D. de Certaines, *Magn. Reson. Imaging* 17(9), 1393 (1999).
48. F. Lefebvre, M. Meunier, F. Thibault, P. Laugier and G. Berger, *Ultrasound Med. Biol.* 26(9), 1421 (2000).
49. D. Chappard, A. Chennebault, M. Moreau, E. Legrand, M. Audran and M.F. Basle, *Bone* 28(1), 72 (2001).
50. M.F. McNitt-Gray, N. Wyckoff, J.W. Sayre, J.G. Goldin and D.R. Aberle, *Comput. Med. Imag. Grap.* 23, 339 (1999).
51. D.G. Vince, K.J. Dixon, R.M. Cothren and J.F. Cornhill, *Comput. Med. Imag. Grap.* 24, 221 (2000).
52. J. Bézy-Wendling and M. Krętowski, *Proc. of ISBI'02*, 141 (2002).
53. M. Krętowski and J. Bézy-Wendling, *Biocybernetics and Biomedical Engineering* 23(1), 65 (2003).